Original Article

Institution of MECHANICAL ENGINEERS
Journal of ENGINEERING MANUFACTURE

Proc IMechE Part B:
J Engineering Manufacture
2024, Vol. 238(4) 577–589

DOI: 10.1177/09544054231166461
journals.sagepub.com/home/pib
SAGE

Performance of cutting-tool patterns textured via ultrashort laser pulses in the turning of martensitic stainless steel under dry and lubricated conditions

Tatiana Dias Santana[1], Wagner de Rossi[2], Patrícia Alves Barbosa[3] and Marcelo Bertolete[1,3]

Abstract

The pulse length for ultrashort pulse lasers is considered shorter than the thermal vibration period of the material lattice. The thermal diffusion depth is negligible when compared with the optical penetration depth because laser-matter interaction occurs only near the focal volume. Hence, ultrashort pulse lasers are indicated for micromachining. This study aims to evaluate straight and zig-zag texture patterns generated by ultrashort laser pulses on the rake face of uncoated cemented carbide tools during the turning of martensitic stainless steel. The tests were performed under dry and lubricated conditions. The output variables were machining force, cutting power, chip thickness ratio and aspects of workpiece quality (form tolerance and surface roughness). The textures presented micrometric dimensions with a narrow deviation. The main results showed that the straight texture pattern decreased the machining force by 17.5% when compared to the zig-zag pattern. For cutting power, the straight pattern reduced consumption by 5.8% and 6.9% in relation to the reference and zig-zag tools, respectively. Finally, under dry machining conditions, the straight tool was able to decrease the workpiece cylindricity deviation by an average of 108% and 25% compared to the reference and zig-zag tools. The results provide evidence that texturing can affect the tribological system, chip-tool interface, with a potential impact on the sustainability of the process.

Keywords

Ultrashort pulse laser, texturing, machining force, cutting power, workpiece quality

Date received: 24 April 2022; accepted: 12 March 2023

Introduction

Ultrashort pulse lasers are laser systems that emit pulses whose temporal duration varies from femtoseconds ($1\,fs = 10^{-15}\,s$) to a few tens of picoseconds ($1\,ps = 10^{-12}\,s$).[1] These systems can generate tens to hundreds of microjoules in a pulse length of 100 fs and peak intensities of approximately $10^{14} - 10^{16}\,W/cm^2$ for focused beams. This implies that the ionisation of virtually any target material occurs at the beginning of the laser pulse time.[2]

When the laser is focused on a metallic material, the free electrons in the skin layer absorb the energy of photons at approximately 1 fs. The relaxation time of the electrons is approximately 1 ps, after which energy is converted into heat. The heat diffuses towards the bulk, in which the diffusion depth is dependent on the material's thermal diffusivity and diffusion time. Then, a pulse can be considered ultrashort when the thermal diffusion depth is of the same order or less than the optical penetration depth (skin layer), which is dependent on the material and laser wavelength. For the

[1]Escola de Engenharia de São Carlos, Universidade de São Paulo, São Carlos/SP, Brazil
[2]Centro de Lasers e Aplicações, Instituto de Pesquisas Energéticas e Nucleares, São Paulo/SP, Brazil
[3]Departamento de Engenharia Mecânica, Universidade Federal do Espírito Santo, Vitória/ES, Brazil

Corresponding author:
M Bertolete, Departamento de Engenharia Mecânica, Universidade Federal do Espírito Santo, Av. Fernando Ferrari, 514, Goiabeiras, Vitória/ES 29075-910, Brazil.
Email: marcelo.b.carneiro@ufes.br

steels, the diffusion depth for 1 ps is approximately 10 nm. Thus, an ultrashort pulse of shorter than 1 and 10 ps can be considered for metals and ceramics, respectively.[3]

For femtosecond lasers, the pulse duration is shorter than the thermal vibration period of the material lattice. Given that the energy deposition is very fast, the amount of molten material and the heat-affected zone are negligible.[4] Wang et al.[5] stated that the advantage of ultrashort pulse lasers is the ability to produce a very high peak power intensity and deliver energy to the material before thermal diffusion occurs.

Owing to the nonlinear excitation mechanism, appropriately focused ultrashort pulses generate strong absorption. Thus, the laser-matter interaction occurs only at the focal volume, which in turn leads to a thermal diffusion length close to the optical penetration depth (thermal effect suppression). Additionally, the peak intensity is sufficiently high to induce multiphoton absorption, which allows the machining of any solid material.[1] Therefore, ultrashort pulse lasers have been widely used for micromachining applications at micrometre and submicrometre scales with better quality and accuracy when compared to those of nanosecond and picosecond pulse lasers.[4,6]

Laser surface texturing (LST) is a fabrication technique that can remove material to create patterned microstructures on a surface.[7,8] Texturing has been examined as a method for controlling tribological, optical, and mechanical properties.[9,10] As for tribological improvements, LST has been used to store lubricants or entrap wear debris, control friction, increase load capacity, enhance wear resistance (extend the lifetime of components), and, in successful cases, address sustainability aspects by saving material resources, energy and enhance operational safety.[11–13]

LST has been applied in cutting tools to improve lubrication at the tool-chip interface, coating adhesion, and for increasing the cutting tool performance. Xing et al.[14] used a nanosecond laser for texturing straight and zig-zag patterns on the rake face of an Al_2O_3-TiC ceramic cutting tool. Furthermore, MoS_2 solid lubricant was burnished into textures. The main output variables that were monitored included the cutting force, cutting temperature, and surface roughness of the AISI 1045 hardened workpiece after turning. Khani et al.[15] textured micro-hole with fibre laser on the rake face of carbide tools and also embedded them with solid lubricants (MoS_2 and carbon nanotube). They monitored the cutting force when thread turning aluminium 7075-T6 alloy. Zhang et al.[12] textured with a nanosecond laser straight pattern on the rake face of cemented carbide tools, and applied TiAlN coating on textured and non-textured tools. They assessed the cutting force, coefficient of friction, and surface roughness of an AISI 1045 hardened workpiece, under dry and lubricated turning conditions. Vasumathy and Meena[16] textured straight patterns with a picosecond laser on the rake face of an uncoated cemented carbide tool at four different positions relative to the cutting edge. The main variables evaluated were the cutting force and chip morphology during the dry-turning operation of AISI 316. Bertolete et al.[17] textured straight patterns on the rake face of cemented carbide tools using a femtosecond laser. They evaluated the machining force, chip features and surface roughness of dry-turning martensitic stainless steel. Wang et al.[18] textured the rake face of monocrystalline diamond tools using a femtosecond laser and performed tribological and machining tests. The main output variables monitored were the friction coefficient, cutting forces and surface roughness of the oxygen-free copper workpiece after turning. Duan et al.[19] produced multiscale textures using a femtosecond laser on the rake face of an Al_2O_3-TiC ceramic cutting tool. The authors monitored the cutting forces, cutting temperature, and tool wear after turning the AISI H13 under conventional lubrication conditions. All of the aforementioned studies were generally successful with textured cutting tools. However, there is a paucity of scientific studies involving texturing of cutting tools to evaluate the machining force, form tolerance and relate the output variables with sustainability aspects when considering stainless steel machining.[20]

Therefore, this study involved evaluating straight and zig-zag texture patterns produced by ultrashort laser pulses on the rake face of uncoated cemented carbide tools during the turning of martensitic stainless steel under medium cutting conditions with or without cutting fluid. The texture dimensional aspects were characterised. Furthermore, the influence of the cutting-tool patterns on the machining force, cutting power, chip thickness ratio and workpiece quality (form tolerance and surface roughness) was characterised. Finally, comments on the performance of the textured cutting tool and sustainability were presented.

Materials and methods

Tungsten cemented carbide tools with geometry TPUN 160304, BA55 grade (Brassinter), were textured on the rake face with a parallel orientation and 260 μm from the main cutting edge. Two groove patterns were produced, straight and zig-zag, as shown in Figure 1. The inserts did not contain chipbreakers and the flat surface, before texturing, presented arithmetic average surface roughness (Ra) of 0.166 ± 0.038 μm. Dimensions and orientation of textures were based on literature[13,14,21] and empirical observations aiming to enhance tribological aspect at tool-chip interface to decrease cutting forces and improve geometrical tolerancing.

According to the cutting-tool manufacturer, BA55 corresponds to a P25/P45 ISO grade and is recommended for machining stainless steel. This insert is justified by being one of the few uncoated tools available in the market, which is capable of machining at workpiece. Thus, the results were only influenced by the

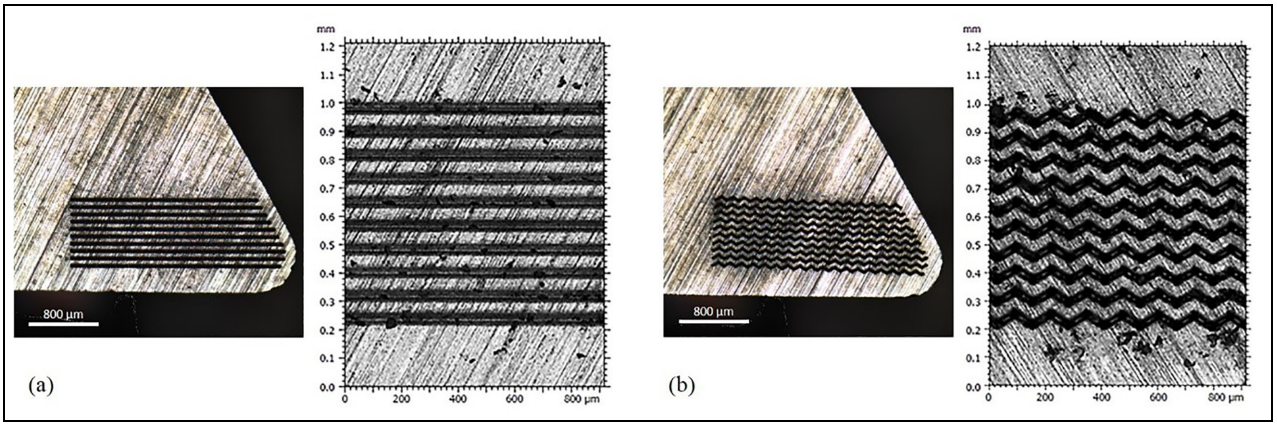

Figure 1. Texture patterns applied on the rake face of TPUN 160304 cutting tool: (a) straight and (b) zig-zag.

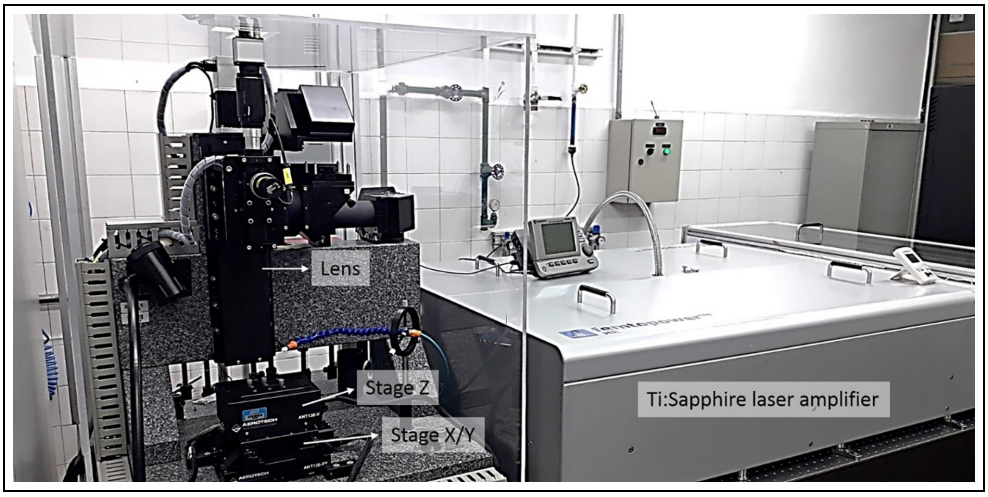

Figure 2. Ultrashort laser system composed of amplifier, lens train and XYZ stages.

presence or absence of texture in the cutting-tool interface. The tools were mounted on a CTGPR 2525 M16 (Sandvik) tool holder, which allowed a semi-orthogonal cutting geometry with a cutting-edge angle (κ_r) of 91°, cutting-edge inclination angle (λ_s) of 0°, and clearance angle (α) of 5°.

The cutting tools were textured by ultrashort laser pulses in a workstation that uses a Ti:Sapphire laser, model HR Femtopower (Femtolasers), as shown in Figure 2. The emission wavelength were centred at 785 µm with a bandwidth of 110 nm, pulse duration of 30 fs pulses, repetition rate of 10 kHz and energy of 4 µJ. The laser beam was focused on the rake face of the tools by using a lens with a focal length of 20 mm. The focus spot size ($\varnothing_f$) was approximately 3.1 µm, as calculated by equation (1), where M^2 denotes the beam quality factor of 1.4, f represents the focal length, λ the laser wavelength and $\varnothing_0$ means the beam diameter at the lens entrance of 9 mm.

Texture dimensions, such as depth, width and pitch, were evaluated in a 3D optical microscope, CM Explorer (Mahr), using a 50× magnification lens. The textured area was divided into three parts: the left, middle and right. Each part allowed 10 observations; thus, three average values of the texture dimensional aspects were obtained for each textured region.

$$\varnothing_f = \frac{4M^2 f\lambda}{\pi\phi_0} \quad (1)$$

The workpiece was martensitic stainless steel VSM 13 (Villares Metals) with a Vickers hardness number of 274 HV30, diameter of 62 mm and length of 160 mm. Three bars were used for the machining tests. About 2 bars were used for textured tools and 1 bar was used for the reference cutting tool (non-textured). For statistical assumptions, the bars will be considered equal and the fixation will not influence the results. The runout deviation was inferior to 5 µm. The tests were conducted in a CNC lathe Centur 35D (Romi). The cutting parameters were maintained as constant at a cutting

Table 1. Input variables for the machining tests.

Cutting-tool patterns	Cutting conditions	Lubrication condition
Straight texture Zig-zag texture Reference (non-texture)	v_c = 100 m/min f = 0.2 mm/rev a_p = 2 mm	Dry and lubricated

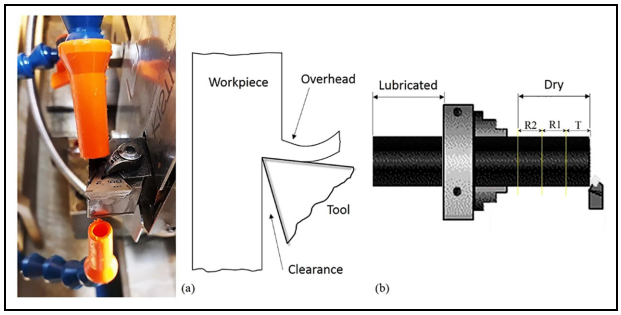

Figure 3. Experimental details: (a) direction of cutting fluid application and (b) machining test scheme on the workpiece.

speed (v_c) of 100 m/min, feed rate (f) of 0.2 mm/rev, and depth of cut (a_p) of 2 mm. However, machining was realised under dry and lubricated conditions, as listed in Table 1. The cutting fluid corresponded to a semisynthetic LESS BIO100 (Lubless) with 10% concentration. The cutting fluid was conventionally applied along the side clearance and on the back of the chip (overhead), at a flow rate of 5 l/min. Thus, the martensitic stainless steel bars were machined in half under dry conditions and in the other half under lubricated conditions. Given that the insert had a triangular form with three cutting edges, each machining test was performed once (T) with two replications (R1 and R2), using a new edge, as shown in Figure 3. The feed length (Lf) was set as 20 mm.

During the machining tests, three orthogonal force components (F_x, F_y and F_z) acting on the cutting tool were monitored. Based on this, the machining force or resultant force (F_R) in Newtons was calculated using equation (2), and the cutting power (P_c) in kilowatts was estimated using equation (3), wherein $F_y = F_c$ (cutting force) in the v_c direction. The orthogonal force components were measured with the aid of a dynamometric system composed of a piezoelectric platform (model 9129), signal conditioner (model 5080A) and data acquisition system (model 5697A1, Kistler), as shown in Figure 4. The data acquisition for each test and replication was 1000 kHz. Three observations (T, R1 and R2) comprised the average values of the machining force and cutting power for the specific cutting-tool patterns. Furthermore, the chip thickness ratio (r) was also measured as the ratio between the deformed (h') and undeformed (h) chip thicknesses, as shown in equation (4). An external electronic micrometre with a measuring range of 0–25 mm, resolution of 0.001 mm, accuracy of ±0.002 mm and a spherical tip device (Digimess) was used to measure h'. The feed rate value was considered for h. Three observations (T, R1 and R2) comprised the average values; however, each value was obtained from 12 assessments.

$$F_R = \sqrt{F_x^2 + F_y^2 + F_z^2} \tag{2}$$

$$P_c = \frac{F_c v_c}{6.10^4} \tag{3}$$

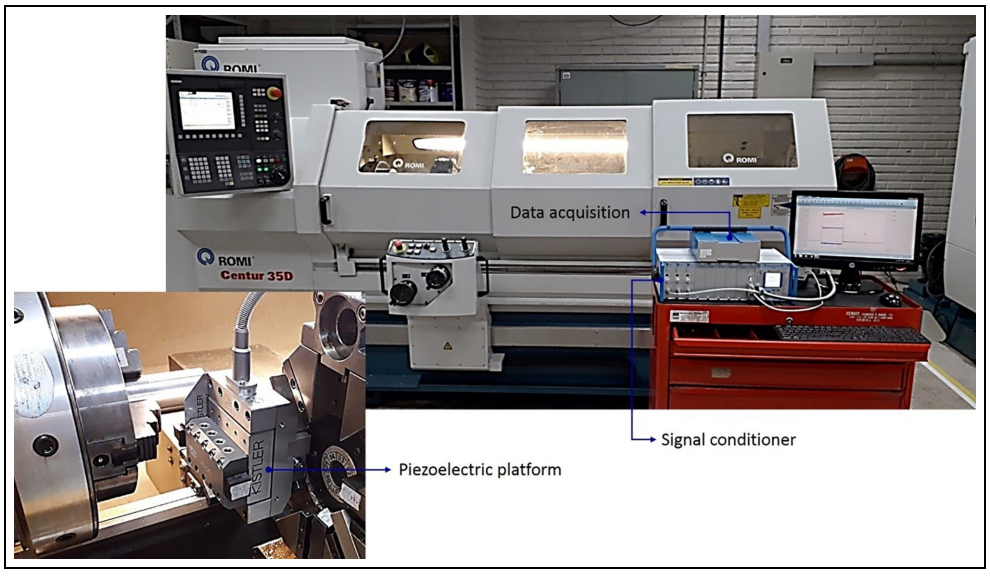

Figure 4. Dynamometric system composed of a piezoelectric platform, signal conditioner and data acquisition system. The CNC lathe can be observed in the background.

Table 2. Characterisation of texture patterns.

	Straight texture			Zig-zag texture		
	Depth	Width	Pitch	Depth	Width	Pitch
N	18	18	18	18	18	18
Mean (μm)	9.05	25.83	80.18	12.33	25.02	80.02
CI−95% (μm)	8.37	24.93	80.00	11.42	24.53	79.81
CI + 95% (μm)	9.73	26.73	80.36	13.24	25.52	80.24
Std. dev. (μm)	1.37	1.82	0.36	1.83	0.99	0.42

$$r = \frac{h'}{h} \tag{4}$$

A scanning electron microscope (SEM), Quanta FEG650 (FEI), equipped with an energy-dispersive spectrometer (EDS), Quantax (Bruker), was used after the machining test to investigate the adherence of the workpiece material on the rake face of the cutting tools.

Additionally, form tolerance was evaluated by measuring cylindricity. Hence, measurements were conducted at five different positions, 2 mm apart, in each experimental region (T, R1 and R2). Three average values (observations) comprised the cylindricity results generated by a specific cutting-tool pattern. A universal form tester, MMQ 400-2 (Mahr), was used. The least-square centre with a waviness filtre 150 of UPR (Undulations per Revolution) was used according to ISO 1101:2017.[22] Furthermore, the surface finish, considering the surface roughness parameters Ra (arithmetic average height), was also measured via a roughness tester, MarSurf PS 10 (Mahr), with a cut-off set at 0.8 mm according to ISO 21920-3:2021.[23] The measurements were performed for testing and replication at arbitrary bar positions of 0°, 90°, 180° and 270°. Surface roughness results were obtained from the average values of the three experimental regions.

Results and discussions

Texture characterisation was first introduced to specify the dimensional aspects. The results were evaluated using descriptive statistics. Next, the effect of the cutting-tool patterns on the machining and workpiece finishing results was presented. In this case, the data were evaluated using two-way analysis of variance (ANOVA) with interactive effects.

Texture characterisation

The characterisation of the texture using a non-contact microscope is useful in assessing the dimensions of texture patterns and correlates with the capacity of the laser manufacturing process. Table 2 shows a descriptive statistical analysis for straight and zig-zag textures, considering the depth and width, as well as the pitch between grooves. Eighteen observations were used for the analysis, as a new textured tool was used for dry and lubricated machining.

The texture aspects (depth, width and pitch) exhibited a narrow standard deviation and 95% confidence interval. The difference between the average values for straight and zig-zag textures was only 3.28, 0.81, and 0.19 μm in terms of depth, width and pitch, respectively. These results converged to the characteristics of ultrashort pulse lasers, which promoted micromachining with extremely accurate dimensions. As the laser pulse duration is quite short and the peak intensity is extremely high, the ultrashort pulse interaction with matter is nonlinear. This in turn leads to the generation of a tightly focused light field with strong absorption that can remove material only close to the focal volume, which defines precise ablation thresholds.[1,3] Furthermore, the precision of the CNC stages, in the micrometre to nanometre range, contributes to improving the machining accuracy as observed in the pitch dispersion values. Based on the analysis using a confocal microscope (Figure 5), it was possible to identify 'v' form of the groove. This explanation is associated with the Gaussian profile of the spatial energy distribution, which is higher at the centre and minimum at the border.

Dimensional aspects of the texture, including grooves orientation, distance from the main cutting edge, and texture length from the tip-tool, combine to influence lubricant storage or debris retention, which can subtly change the chip formation and movement at the tool-chip interface.

Machining results

Table 3 shows machining force (F_R) values for the test (T) and replications (R1 and R2) by considering two textured tools (straight and zig-zag patterns) and one reference tool (non-textured) in the lubrication condition (dry and lubricated).

Table 4 presents the ANOVA for the machining force results. The level of statistical significance (α) for the hypothesis test was 5% (or 0.05) using Fisher's distribution (F). SS represents the residual sum of squares. MS denotes the mean square (or variance). F is calculated by the ratio of variances, source of variation (factors) and error. The p-values are calculated from F to be compared with α. It was observed that there was a

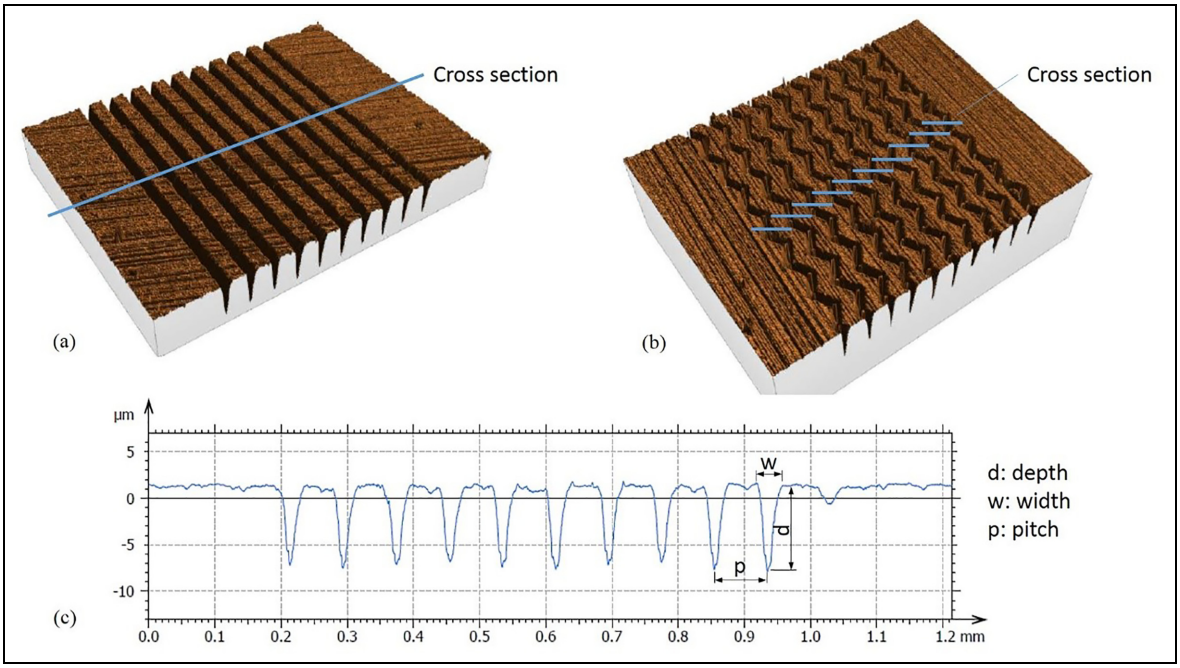

Figure 5. Cross sectional: (a) straight texture, (b) zig-zag texture and (c) representative 'v' form profile and dimensional aspect observed for both texture patterns.

Table 3. Machining force (F_R) results.

Cutting tool	Lubrication condition	T (N)	R1 (N)	R2 (N)
Straight	Dry	1237.38	1390.09	1042.36
	Lubricated	1174.48	1182.65	1199.13
Zig-zag	Dry	1638.49	1446.44	1507.04
	Lubricated	1517.14	1244.28	1407.22
Reference	Dry	1136.38	1255.70	1453.90
	Lubricated	1437.16	1232.46	1349.40

Table 4. ANOVA for results of machining force.

Effect	SS	Degrees of freedom	MS	*F*	*p*
Intercept	31,605,750	1	31,605,750	1990.031	0.000000
Tool	198,057	2	99,028	6.235	0.013907
Lubrication	7355	1	7355	0.463	0.509091
Tool × Lubrication	29,652	2	14,826	0.934	0.419939
Error	190,585	12	15,882		

significant difference among tools ($p < \alpha$); however, lubrication condition and interaction between variables were not significant ($p > \alpha$).

Figure 6(a) shows that texturing influences the machining force. It was observed that the straight texture pattern decreased the response by an average of 17.5% and 8.1% when compared to the zig-zag texture pattern and reference tool, respectively. Thus, a significant difference between straight and zig-zag texture patterns is identified. However, there were no significant differences between the straight pattern and reference tool or between the zig-zag pattern and reference tool. Finally, on average, the F_R results for the zig-zag tool were 11.4% greater than those of the reference. Although the interaction, Tool × Lubrication, is not significant, the results in Figure 6(b) suggest that the cutting fluid can potentially affect the zig-zag pattern to a higher extent because the decrease in the rate of force was higher than that of the other tools. For the straight texture tool and reference tool, the cutting fluid did not influence the response (F_R) in the given experimental cutting conditions.

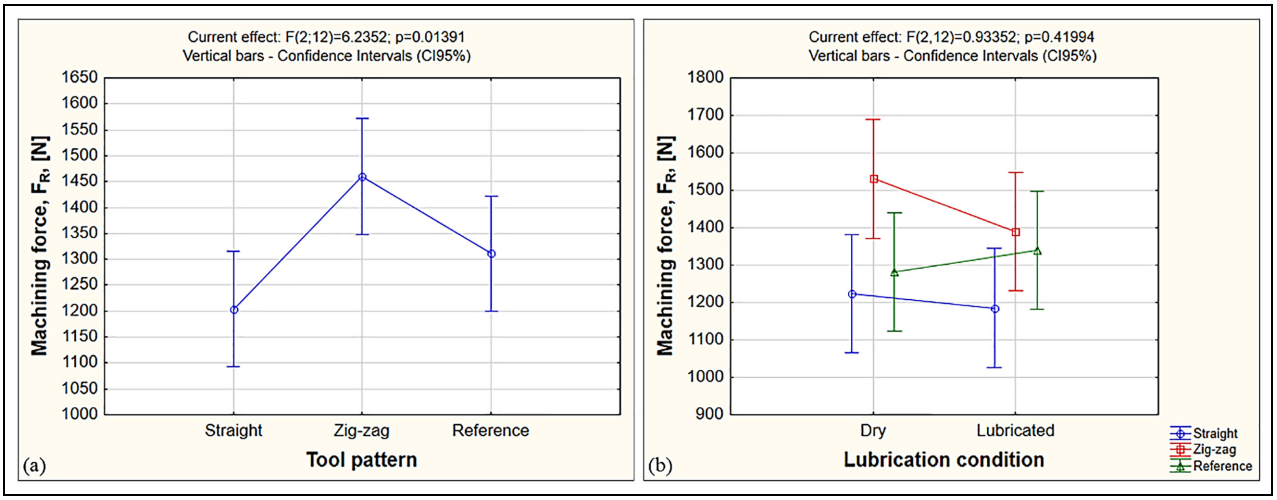

Figure 6. Machining force: (a) tool effect and (b) interaction effect (Tool × Lubrication).

Table 5. Cutting power (P_c) results.

Cutting tool	Lubrication condition	T (kW)	R1 (kW)	R2 (kW)
Straight	Dry	1.58	1.59	1.49
	Lubricated	1.67	1.71	1.72
Zig-zag	Dry	1.69	1.58	1.62
	Lubricated	1.89	1.76	1.95
Reference	Dry	1.57	1.68	1.71
	Lubricated	1.82	1.74	1.80

Table 6. ANOVA for cutting power results.

Effect	SS	Degrees of freedom	MS	*F*	*p*
Intercept	51.84798	1	51.84798	13,468.93	0.000000
Tool	0.04767	2	0.023'84	6.19	0.014207
Lubrication	0.13542	1	0.13542	35.18	0.000069
Tool × Lubrication	0.01009	2	0.00504	1.31	0.305732
Error	0.04619	12	0.00385		

Zhang et al.[12] observed a reduction in cutting forces of 21%–34% for cemented carbide cutting tools with texture parallel to the cutting edge and coated with TiNAl, mainly under lubricated conditions, after turning hardened AISI 1045 steel in finish cutting conditions. Vasumathy and Meena[16] textured cemented carbides using different patterns. They observed better results for straight textures parallel to the cutting edge, with a cutting force reduction of 7.7%, after turning AISI 316 under medium- and dry-cutting conditions. Hao et al.[24] textured straight patterns and a combination of straight and zig-zag patterns, and both were parallel to the cutting edge of cemented carbide tools. The authors turned Ti6Al4V under finish cutting conditions to dry and minimum quantity lubrication. The cutting force results were similar to those of the tested cutting tools irrespective of the lubrication condition. Bertolete et al.[17] reported a 20% reduction in machining force for the best model of straight texture patterns when compared to the reference tool after turning in medium-condition martensitic stainless steel. The variability in the cutting forces results is related to the different texture dimensions, density distribution and texture orientation in relation to the chip flow, as well as different cutting tool and workpiece materials.

Table 5 lists cutting power (P_c) values for the test (T) and replications (R1 and R2) by considering the cutting-tool patterns and lubrication condition.

Table 6 shows the ANOVA results for the cutting power. The significance level (α) was 5% (or 0.05). The main variables, Tool and Lubrication, were statistically significant, as opposed to the interaction.

Figure 7 shows the effects of the variables on the response. Figure 7(a) shows the tool effect, in which

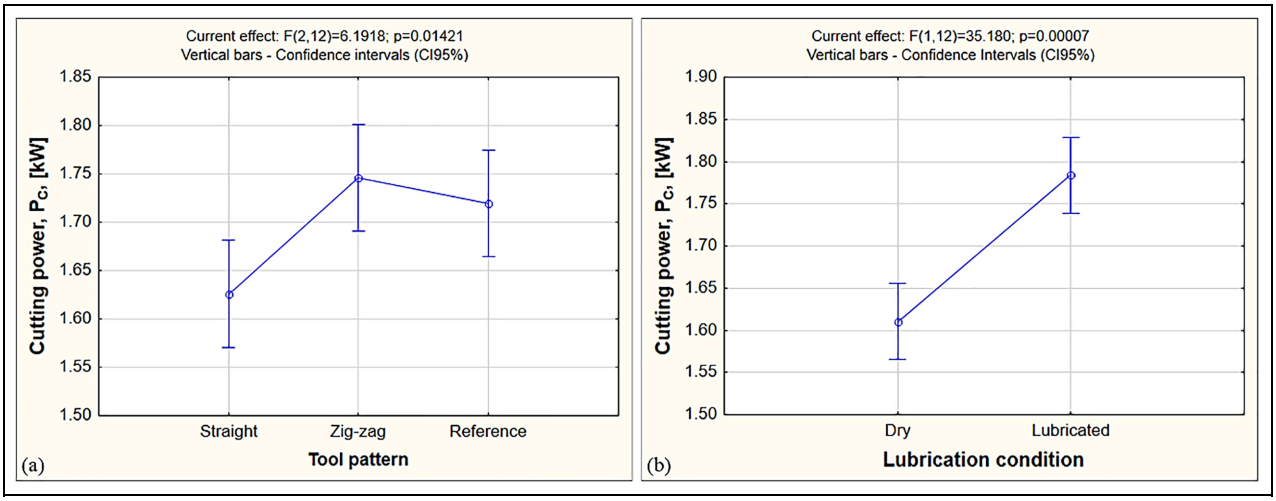

Figure 7. Cutting power: (a) tool effect and (b) lubrication effect.

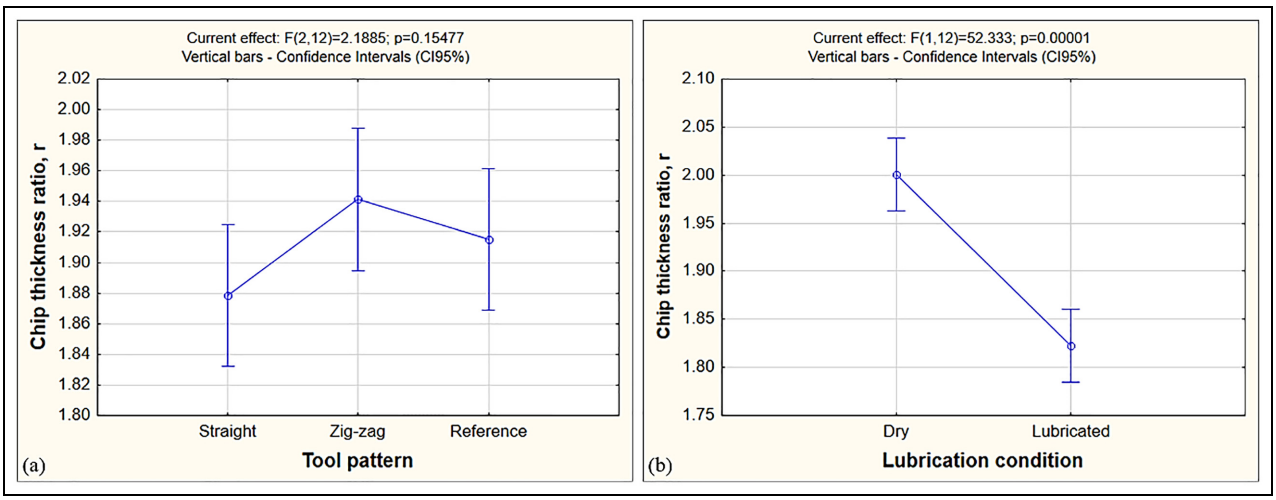

Figure 8. Chip thickness ratio (r): (a) tool effect and (b) lubrication effect.

the straight pattern texture allowed significantly lower cutting power than the zig-zag and reference tools, with an average decrease of 6.9% (0.12 kW) and 5.8% (0.09 kW), respectively. Then, it is evident that the texture pattern can affect the tribological system at the cutting-tool interface. Figure 7(b) shows that the cutting fluid significantly increases the cutting power by 10.8% (0.17 kW). In certain situations during metal cutting, the heating effect generated by shearing the material is more intense than that of strain hardening. This leads to thermal softening of the material, loss of strength, decrease in cutting force (F_c) and, consequently, cutting power (P_c). It is important to note that the power consumption of the hydraulic pump was disregarded from the estimate, that is, the difference must be higher. If the texture pattern causes a decrease in F_c and P_c, then it implies that the shear planes are changing, and the assessment of chip thickness ratio (r) can verify this.

By analysing Figure 8(a), assessment of the chip thickness ratio (r), it is noted that the chip generated by the straight texture is on average 3.2% and 1.9% thinner than the zig-zag and reference patterns, respectively. This difference was not statistically significant at the 5% significance level (α). However, by considering an error probability of approximately 15%, which is not absurd in machining owing to the variability in the process, the straight texture can potentially decrease F_c and P_c, with decreasing shear plane areas and consequently the chip thickness. Figure 8(b) shows that the cutting fluid has a strong effect on reducing the chip thickness ratio (8.9%). However, this occurs with a significant increase in the cutting power, as shown in Figure 7(b), owing to the cooling action of the cutting fluid, which reduces the thermal softening effect in the material caused by plastic deformation during chip formation. Kawasegi et al.[9] observed variation in the shear angle and, consequently, in the chip thickness

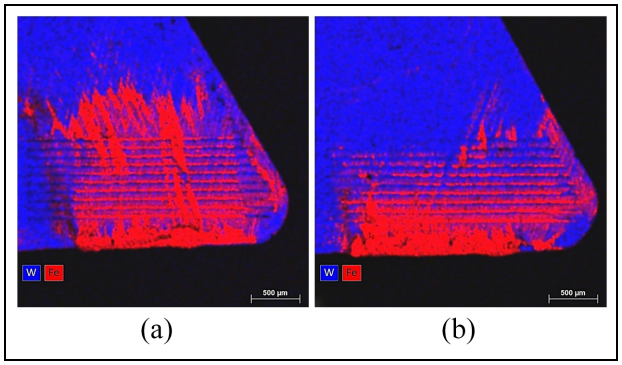

Figure 9. SEM-EDS rake face images for the tools with straight texture: (a) dry condition and (b) lubricated condition.

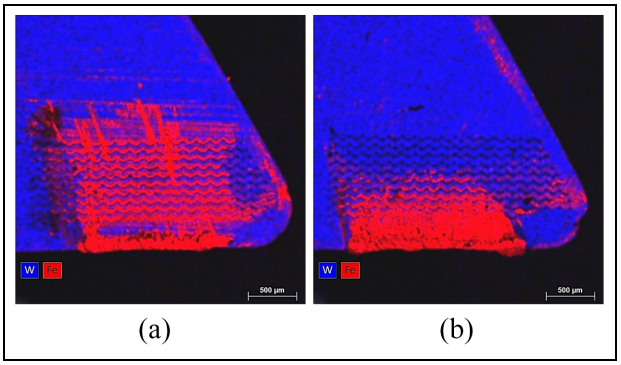

Figure 10. SEM-EDS rake face images for the tools with zig-zag texture: (a) dry condition and (b) lubricated condition.

ratio, for the nanotextured cutting tool in the turning aluminium alloy A5052. Xie et al.[21] observed the shear angle changing with the depth of the microgroove when turning Ti-6Al-4V. Kim et al.[25] reported lower chip thickness ratio values for the microtextured tools than for the reference tool at different feed rates when turning 52100 hardened steel.

Figures 9–11 show SEM images with chemical elements detected by EDS on the rake face of the cutting tools tested under dry and lubricated conditions. Blue and red denote tungsten carbide (W) of the tools and iron (Fe) of the workpiece material, respectively. Figure 9(a) shows that the workpiece material (Fe) adheres close to the main cutting edge of the straight-textured tool. This area can be distinguished as a sticking zone. Next, it was observed that the workpiece material adhered inside the grooves, and the adhered material, with a signal of relative motion, can be considered as the sliding zone. As shown in Figure 9(b), the cutting fluid decreases the tool-chip contact area around 30%, which leads to a slight decrease in the machining force and a thinner chip thickness when compared to the dry-cutting condition, as shown in Figure 6(b). This effect is likely related to the mixed or boundary lubrication regimes, as reported by Gachot et al.,[7] in which textures can retain cutting fluid or a tribochemical reaction layer is formed around them. However, the decrease in the contact area did not imply lower cutting power.

Figure 10(a) shows that the workpiece material (Fe) adheres close to the main cutting edge on the tool rake face with a zig-zag texture. This region must be considered a sticking zone. After that, there is adhered material inside the zig-zag grooves, in addition to the adhered material with a signal of a relative motion suggesting the sliding zone. The texture pattern and amount of material adhered to the texture can explain the difference in behaviour between the straight and zig-zag textures. Figure 9(a) suggests the presence of more adhered material in this texture pattern. As shown in Figure 10(b), the cutting fluid decreases the tool-chip contact area by 50%, making it difficult to distinguish between the sticking and sliding zones, as the adhered workpiece material extends towards the textured

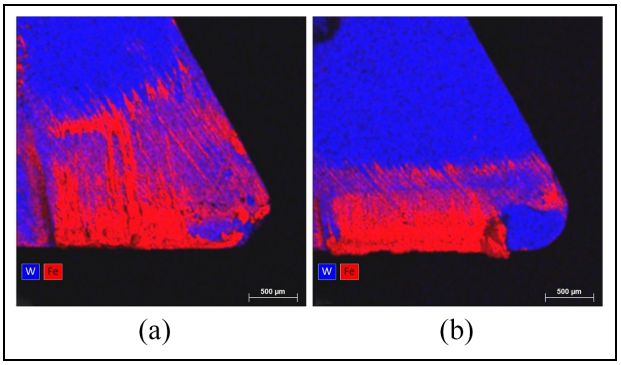

Figure 11. SEM-EDS rake face images for the reference tools: (a) dry condition and (b) lubricated condition.

region. Thus, the shorter contact area decreased the machining force and chip thickness in relation to dry cutting. However, this did not influence the cutting power. When compared to straight and zig-zag textures under lubricated conditions, the contact region for the former tool was wider than that for the latter, because more workpiece material was trapped inside the grooves. This can potentially be considered as evidence of superior performance of the former. Finally, the zig-zag cutting tool spalled at the corner radius under lubricated conditions. This fracture may have been caused by a combination of mechanical and thermal cracks close to the tool tip. Thermal cracks are justified owing to the cutting fluid.

Figure 11(a) shows a sticking zone, close to the main cutting edge, twice as large as that of the straight texture under the same dry-cutting conditions. Furthermore, spalling occurs in the corner rounding of the reference tool. In this case, justified only by mechanical loading. The best performance of the straight-textured tool can be associated with the clogging effect. The adhered material or debris trapped in the grooves forms a sufficiently thick layer capable of reducing load, coefficient of friction, wear rate and abrasivity.[26,27] Successful texturing is dependent on the texture geometry, dimension (or aspect ratio), surface

Table 7. Cylindricity deviation results.

Cutting tool	Lubrication condition	T (μm)	R1 (μm)	R2 (μm)
Straight	Dry	21.377	18.207	16.460
	Lubricated	29.434	29.124	24.424
Zig-zag	Dry	32.571	20.889	21.903
	Lubricated	38.268	25.765	23.136
Reference	Dry	41.057	44.428	31.476
	Lubricated	30.490	29.195	21.297

Table 8. ANOVA for cylindricity deviation results.

Effect	SS	Degrees of freedom	MS	*F*	*p*
Intercept	13,861.11	1	13,861.11	434.8497	0.000000
Tool	293.20	2	146.60	4.5991	0.032907
Lubrication	0.42	1	0.42	0.0133	0.910031
Tool × Lubrication	359.50	2	179.75	5.6392	0.018766
Error	382.51	12	31.88		

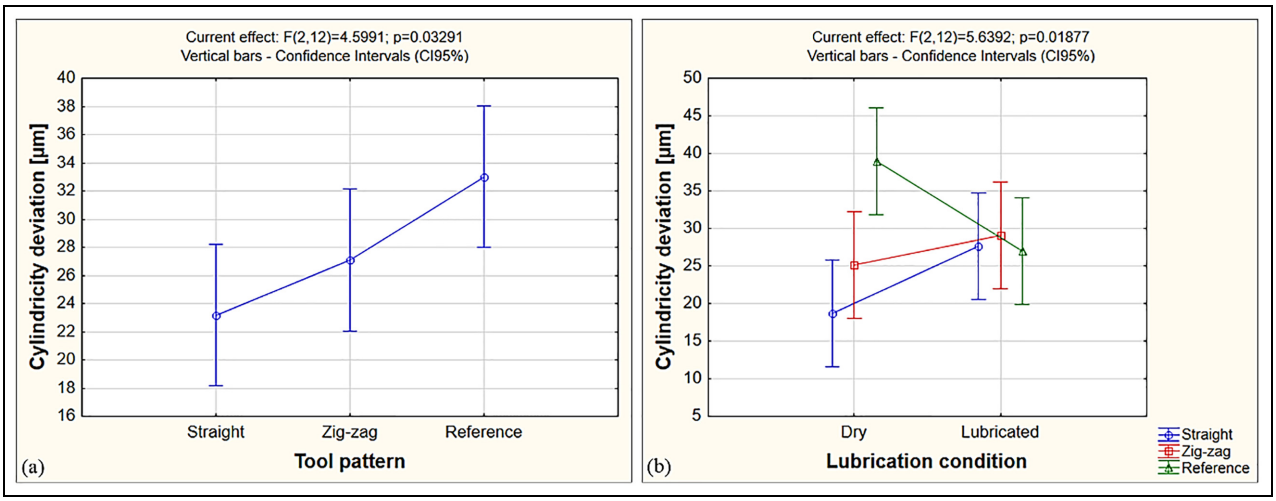

Figure 12. Cylindricity deviation: (a) tool pattern effect and (b) tool pattern and lubrication condition interaction effect.

density and relative orientation between the texture and chip movement.[7,13] Xie et al.[21] reported lower cutting temperate and, consequently, less tool wear when turning titanium with a microtextured tool. Kim et al.[25] cited flank wear reduction of 11% for textured tool; in addition, they mentioned abrasion, adhesion, and diffusion as wear mechanisms in hard turning of AISI52100. Observing the workpiece material adhered on the textured rake face, attrition wear mechanism is expected to occur throughout the tool life. In Figure 11(b), the cutting fluid decreases the tool-chip contact area by 31%. It can distinguish the sticking zone from the main cutting edge and, subsequently, the sliding zone with the relative motion signal of the adhered material. On the rake face, the corner radius exhibited spalling. Probably, caused by mechanical loading and thermal shock due to the cutting fluid used. Despite the smaller contact area, except for the chip thickness ratio, the cutting fluid led to an increase in the machining force and power cutting.

Workpiece finishing results

Table 7 lists the cylindricity form deviation (⌭) values for the test (T) and replications (R1 and R2).

Table 8 presents the ANOVA for the cylindricity deviation results at a significance level (α) of 5%. There was a statistically significant interaction between the Tool and Lubrication.

Figure 12(a) shows the effect of the main variable, Tool, without considering the lubrication effect. It is observed that the straight-texture tool provides

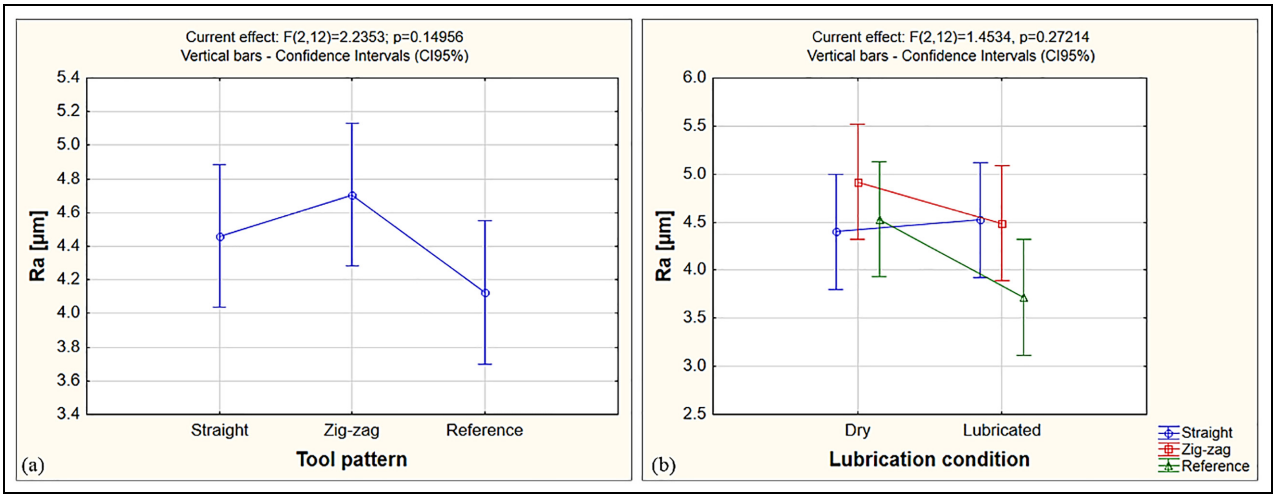

Figure 13. Surface roughness, evaluated parameter Ra: (a) tool pattern effect and (b) tool pattern and lubrication condition interaction effect.

cylindricity deviation values that are statistically lower than the reference values. The analysis was more accurate when the interaction was considered, as can be seen in Figure 12(b). In this case, the lubricated condition for the textured tools did not improve the workpiece quality, which was contrary to the case of the reference. For the lubricated condition, the cylindricity results were extremely similar for different cutting tools. However, in the dry-cutting condition, the results for the textured tools were quite different from those in the reference. The straight-texture pattern decreased the response on average when compared with the reference and zig-zag tools under dry conditions by 108% and 25%, respectively. The zig-zag tool decreased the response under the same conditions by 35% when compared with the reference tool. This can mean fewer scrapped or post-processing parts.

The straight-texture tool provided a lower machining force, cutting power, chip thickness ratio and cylindricity deviation when compared to the other tools. This implies that the straight-textured tool exhibits a strong potential to promote the sustainability of the cutting operation. Researchers in the metal-cutting sector are currently exploring alternatives to minimise environmental impacts and increase efficiency. In this sense, the surface texturing of cutting tools has gained attention.[28] The decrease in the machining force and cutting power might influence tool life, waste management, and energy consumption. Additionally, given that the cutting fluid does not aid the operation under such conditions, it can be eliminated. Consequently, it can lead to a reduction in the Earth's natural resources (water) and energy consumption, lower environmental emissions (effluent disposal) and enhanced operational safety.[29,30] All the sustainability aspects mentioned influence the latter, manufacturing costs. Thus, the five major sustainability metrics can be affected.[31]

When the tool pattern and lubrication conditions were evaluated in terms of the workpiece surface roughness, they did not statistically influence the response at a significance level (α) of 5% or 10%. Figure 13(a) shows the effect of the Tool on the arithmetic average height (Ra parameter). The difference between the Ra values for the straight and reference tools was only 0.34 µm. The calculated significance level (p) was close to 15%; therefore, there was no difference among the tools. The same situation was observed for the lubricated condition. The cutting fluid decreased the average Ra value by 0.37 µm when compared to dry cutting; and, the calculated significance level (p) was 12%. The most interesting result, although statistically insignificant, is the interaction between the Tool and Lubrication, as shown in Figure 13(b). The cutting fluid does not improve the surface roughness generated by the straight tool pattern. Under dry conditions, the difference between the best and worst results was 0.52 µm. Finally, under the lubricated condition, the cutting fluid slightly improved the surface roughness generated by the reference and zig-zag tool pattern. The Ra values of the textured tools were similar. In addition, the difference between the best and worst results was 0.80 µm. Thus, the results reinforce the sustainability of dry machining.

Xing et al.[14] textured straight and zig-zag patterns on the rake face of Al_2O_3-TiC ceramic with nanosecond and femtosecond lasers. They observed the best Ra values for the conventional tool in AISI 1045 turning under finish-cutting conditions. Zhang et al.[12] textured a straight pattern on the rake face of cemented carbide tools using nanosecond laser pulses and coated them with TiAlN. They turned AISI 1045 in finishing cutting conditions and observed better results of Ra in dry and especially in lubricated conditions when compared to the reference tool. Bertolete et al.[17] textured four

different straight patterns on the rake face of cemented carbide tools using ultrashort laser pulses. They turned martensitic stainless steel under medium cutting conditions and observed better Ra values for textured tools. In addition to the dimensional aspects, density and orientation of the textures. Tool and workpiece material, cutting operation and cutting conditions must be considered, as they will influence texture performance.

Conclusions

One of the applications of the femtosecond laser (ultrashort pulse laser) in micromachining was achieved with the fabrication of textures in a high fluence regime with micrometric dimensions, in a 'v' form, on the rake face of cemented cutting tools.

In this sense, the main contribution of this work is to bring new evidence of the effect of texturing on the tribological system, chip-tool interface, with a potential impact on the process sustainability.

As a result, the straight texture pattern decreased the machining force when compared to the zig-zag and reference tools by 17.5% and 8.1%, respectively. While the cutting fluid did not significantly influence this response.

The straight pattern texture provided a statistically significant and lower cutting power than the zig-zag texture pattern (6.9%) and reference (5.8%) tools. In this case, the cutting fluid significantly increased the cutting power by 10.8%.

When the rake face of the cutting tools was analysed using SEM, the cutting fluid provided a shorter tool-chip contact length; however, it was not sufficient to influence the machining force, cutting power, and workpiece finishing results. There was spalling at the corner radius for zig-zag and reference tools, mainly under lubricated conditions.

As for surface roughness, no influence of the input variables (Tools and Lubrication condition) was observed.

Finally, the straight texture tool decreased the cylindricity deviation values under dry conditions by 108% and 25% when compared to the reference and zig-zag tools, respectively.

Considering the results, they suggest that the straight texture tool has strong potential to promote the sustainability of the cutting operation. The best performance is associated with the effects of thermal softening and clogging of the workpiece material in the grooves, forming a tribofilm.

Declaration of conflicting interests

The author(s) declared no potential conflicts of interest with respect to the research, authorship, and/or publication of this article.

Funding

The author(s) disclosed receipt of the following financial support for the research, authorship, and/or publication of this article: The authors would like to thank FAPES (Grants 083/2019 and 144/2020), CNPq and Capes for providing financial support.

ORCID iD

M Bertolete https://orcid.org/0000-0001-5817-8475

References

1. He F, Ni J, Zeng B, et al. Spatiotemporal manipulation of ultrashort pulses for three-dimensional (3-D) laser processing in glass materials. In: Lawrence J and Waugh DG (eds.), *Laser surface engineering: processes and applications*. Cambridge: Woodhead Publishing, 2015, pp.383–404.
2. Gamaly EG, Rode AV, Luther-Davies B, et al. Ablation of solids by femtosecond lasers: ablation mechanism and ablation thresholds for metals and dielectrics. *Phys Plasmas* 2002; 9: 949–957.
3. Meijer J, Du K, Gillner A, et al. Laser machining by short and ultrashort pulses, state of the art and new opportunities in the age of the photons. *CIRP Ann Manuf Technol* 2002; 51: 531–550.
4. Nolte S, Momma C, Jacobs H, et al. Ablation of metals by ultrashort laser pulses. *J Opt Soc Am B* 1997; 14: 2716.
5. Wang XC, Zheng HY, Chu PL, et al. High quality femtosecond laser cutting of alumina substrates. *Opt Lasers Eng* 2010; 48: 657–663.
6. Liang WL, Ngoi BKA, Lim LEN, et al. Micromachining of circular ring microstructure by femtosecond laser pulses. *Opt Laser Technol* 2003; 35: 285–290.
7. Gachot C, Rosenkranz A, Hsu SM, et al. A critical assessment of surface texturing for friction and wear improvement. *Wear* 2017; 372–373: 21–41.
8. Chen P, Xiang X, Shao T, et al. Effect of triangular texture on the tribological performance of die steel with TiN coatings under lubricated sliding condition. *Appl Surf Sci* 2016; 389: 361–368.
9. Kawasegi N, Sugimori H, Morimoto H, et al. Development of cutting tools with microscale and nanoscale textures to improve frictional behavior. *Precis Eng* 2009; 33: 248–254.
10. Fatima A and Mativenga PT. On the comparative cutting performance of nature-inspired structured cutting tool in dry cutting of AISI/SAE 4140. *Proc IMechE, Part B: J Engineering Manufacture* 2017; 231: 1941–1948.
11. Segu DZ, Choi SG, Choi JH, et al. The effect of multi-scale laser textured surface on lubrication regime. *Appl Surf Sci* 2013; 270: 58–63.
12. Zhang K, Deng J, Xing Y, et al. Effect of microscale texture on cutting performance of WC/Co-based TiAlN coated tools under different lubrication conditions. *Appl Surf Sci* 2015; 326: 107–118.
13. Mao B, Siddaiah A, Liao Y, et al. Laser surface texturing and related techniques for enhancing tribological performance of engineering materials: a review. *J Manuf Process* 2020; 53: 153–173.

14. Xing Y, Deng J, Zhao J, et al. Cutting performance and wear mechanism of nanoscale and microscale textured Al2O3/TiC ceramic tools in dry cutting of hardened steel. *Int J Refract Metals Hard Mater* 2014; 43: 46–58.
15. Khani S, Shahabi Haghighi S, Razfar MR, et al. Improvement of thread turning process using micro-hole textured solid-lubricant embedded tools. *Proc IMechE, Part B: J Engineering Manufacture* 2021; 235: 1727–1738.
16. Vasumathy D and Meena A. Influence of micro scale textured tools on tribological properties at tool-chip interface in turning AISI 316 austenitic stainless steel. *Wear* 2017; 376–377: 1747–1758.
17. Bertolete M, Barbosa PA, Machado ÁR, et al. Effects of texturing the rake surfaces of cemented tungsten carbide tools by ultrashort laser pulses in machining of martensitic stainless steel. *Int J Adv Manuf Technol* 2018; 98: 2653–2664.
18. Wang Q, Yang Y, Yao P, et al. Friction and cutting characteristics of micro-textured diamond tools fabricated with femtosecond laser. *Tribol Int* 2021; 154: 106720.
19. Duan R, Wang G and Xing Y. Investigation of novel multiscale textures for the enhancement of the cutting performance of Al2O3/TiC ceramic cutting tools. *Ceram Int* 2022; 48: 3554–3563.
20. Machado AR, da Silva LRR, de Souza FCR, et al. State of the art of tool texturing in machining. *J Mater Process Technol* 2021; 293: 117096.
21. Xie J, Luo MJ, Wu KK, et al. Experimental study on cutting temperature and cutting force in dry turning of titanium alloy using a non-coated micro-grooved tool. *Int J Mach Tools Manuf* 2013; 73: 25–36.
22. International Organization for Standardization. ISO 1101:2017(en), Geometrical product specifications (GPS) — Geometrical tolerancing — Tolerances of form, orientation, location and run-out, https://www.iso.org/obp/ui/#iso:std:iso:1101:ed-4:v1:en (2017, accessed 23 April 2022).
23. International Organization for Standardization. ISO 21920-3:2021(en), Geometrical product specifications (GPS) — Surface texture: Profile — Part 3: Specification operators, https://www.iso.org/obp/ui/#iso:std:iso:21920:-3:ed-1:v1:en (2021, accessed 23 April 2022).
24. Hao X, Chen X, Xiao S, et al. Cutting performance of carbide tools with hybrid texture. *Int J Adv Manuf Technol* 2018; 97: 3547–3556.
25. Kim DM, Lee I, Kim SK, et al. Influence of a micropatterned insert on characteristics of the tool–workpiece interface in a hard turning process. *J Mater Process Technol* 2016; 229: 160–171.
26. Gåhlin R and Jacobson S. The particle size effect in abrasion studied by controlled abrasive surfaces. *Wear* 1999; 224: 118–125.
27. Bijwe J, Indumathi J, John Rajesh J, et al. Friction and wear behavior of polyetherimide composites in various wear modes. *Wear* 2001; 249: 715–726.
28. Pervaiz S, Kannan S, Deiab I, et al. Role of energy consumption, cutting tool and workpiece materials towards environmentally conscious machining: a comprehensive review. *Proc IMechE, Part B: J Engineering Manufacture* 2020; 234: 335–354.
29. Schultheiss F, Zhou J, Gröntoft E, et al. Sustainable machining through increasing the cutting tool utilization. *J Clean Prod* 2013; 59: 298–307.
30. Goindi GS and Sarkar P. Dry machining: a step towards sustainable machining – challenges and future directions. *J Clean Prod* 2017; 165: 1557–1571.
31. Hegab HA, Darras B and Kishawy HA. Towards sustainability assessment of machining processes. *J Clean Prod* 2018; 170: 694–703.